Löwner Based Method for Residual Water Suppression in ^{1}H Magnetic Resonance Spectroscopic Imaging

H. N. Bharath, O. Debals, D. M. Sima, U. Himmelreich, L. De Lathauwer, S. Van Huffel

***Abstract*—Objective: Magnetic resonance spectroscopic imaging (MRSI) signals are often corrupted by residual water and artifacts. Residual water suppression plays an important role in accurate and efficient quantification of metabolites from MRSI. A tensor-based method for suppressing residual water is proposed. Methods: A third-order tensor is constructed by stacking the Löwner matrices corresponding to each MRSI voxel spectrum along the third mode. A canonical polyadic decomposition (CPD) is applied on the tensor to extract the water component, and to subsequently remove it from the original MRSI signals. Results: The performance of the proposed method is demonstrated on both simulated and in-vivo MRSI signals. Conclusion: The tensor-based Löwner method has better performance in suppressing residual water in MRSI signals as compared to the widely-used subspace-based Hankel singular value decomposition (HSVD) method. Significance: Tensor method suppresses residual water simultaneously from all the voxels in the MRSI grid and helps in preventing the failure of the water suppression in single voxels.**

***Index Terms*—Canonical polyadic decomposition, Magnetic resonance spectroscopic imaging, Löwner matrix, Blind source separation.**

I. Introduction

Magnetic resonance spectroscopic imaging (MRSI) is a non-invasive imaging technique that provides spectral profiles in a 2- or 3-D voxel grid, from which the spatial distribution of metabolite concentrations or metabolite ratios can be estimated. Each voxel in the MRSI grid has a spectrum composed of several peaks corresponding to the metabolites present at that location. MRSI has many clinical applications and is used, among others, to investigate psychiatric disorders [1], for diagnosis and prognosis of brain tumors [2], [3], breast cancer [4] and autism [5]. Most of the clinical applications use metabolite concentrations or metabolite ratios obtained from MRSI. Hence, an accurate and efficient quantification of metabolites is important. The metabolite levels in the human tissue are small compared to water, therefore ^{1}H MRSI signals typically contain a large water peak which is usually 10^3 to 10^4 larger than the metabolites of interest. This will affect the quantification of metabolites and has to be suppressed before applying any quantification algorithm. Typically, water suppression techniques are used during the acquisition of MRSI signals to get rid of large water peaks [6]. However, it is difficult to remove the water completely with these methods and some residual water will still be present in the spectra. It is important to suppress the water signal as much as possible for accurate and robust quantification of metabolites.

In general, residual water is suppressed in the preprocessing step using a subspace-based method such as the Hankel singular value decomposition (HSVD) method [7], [8]. In the HSVD method, the water signal is first estimated using a subspace-based decomposition into a sum of complex damped exponentials and subsequently removed from the measured signal to suppress the water component. HSVD is the most popular residual water suppression technique and is available in many software packages such as jMRUI [9], SPID [10], VeSPA [11] and TARQUIN [12] as a preprocessing step before quantification. Other residual water suppression methods based on finite impulse response filter [13] and wavelets [12] are also available in the literature. All these methods suppress water one voxel at a time and do not exploit the shared information present among the voxels in the MRSI grid. As such, the HSVD method might result in poor residual water suppression for some of the voxels in the MRSI grid.

Instead of using matrix-based approaches, there is a trend to convert the matrix data to a higher-order tensor. This transformation is called tensorization, and is part of tensor-based approaches applied on matrix data [14]. Higher-order tensors and their corresponding tools display certain properties that are not available in the matrix domain [15], [16]. Uniqueness of tensor decomposition under mild conditions is one such strong property, where additional constraints are not needed [17], [18].

The water removal from the MRSI signals can be formulated as a blind signal separation (BSS) problem. Recently,

This work was supported in part by Flemish Government FWO project G.0869.12N (Tumor imaging) and G.0830.14N (Block term decompositions), in part by IWT IM 135005, in part by Belgian Federal Science Policy Office: IUAP P7/19 (DYSCO, 'Dynamical systems, control and optimization', 2012-2017), in part by Research Council KUL: CoE PFV/10/002 (OPTEC), in part by EU: European Research Council under the European Union's Seventh Framework Programme (FP7/2007-2013), and in part by EU MC ITN TRANSACT 2012, #316679, and ERC Advanced Grant: BIOTENSORS (n^o 339804). This paper reflects only the author's views and the Union is not liable for any use that may be made of the contained information. This work was also supported by a Ph.D. grant of the Agency for Innovation by Science and Technology (IWT).

H. N. Bharath, O. Debals, D. M. Sima, L. De Lathauwer and S. Van Huffel are with the Department of Electrical Engineering (ESAT), STADIUS Center for Dynamical Systems, Signal Processing and Data Analytics, KU Leuven, Leuven, Belgium (e-mail: bhalandu@esat.kuleuven.be; otto.debals@esat.kuleuven.be; diana.sima@esat.kuleuven.be; sabine.vanhuffel@esat.kuleuven.be).

O. Debals and L. De Lathauwer are also with the Group of Science, Engineering and Technology, KU Leuven Kulak, Kortrijk, Belgium (e-mail: lieven.delathauwer@kuleuven-kulak.be).

U. Himmelreich is with the Biomedical MRI Unit/Molecular Small Animal Imaging Center, Department of Imaging and Pathology, KU Leuven, Leuven, Belgium (e-mail: uwe.himmelreich@med.kuleuven.be).

a Löwner-based BSS method has been developed, which can be used if the source signals can be approximated by rational functions. In this paper, we propose a tensor-based algorithm to suppress the residual water simultaneously from all the voxels in the MRSI signal using this Löwner-based BSS method, under the assumption that the different MRSI components can be well approximated by low-degree rational functions.

This paper is organized as follows: Section II discusses some preliminaries and the Löwner-based blind source separation. The Löwner-based method is then applied in Section III in the MRSI water removal setting. The proposed method is compared with HSVD using simulations and in-vivo-data in Section IV. Some discussions and a conclusion are presented in Section V and Section VI, respectively.

II. Löwner-based blind signal separation

Section II-A introduces tensors and tensor decompositions as part of multilinear algebra and fixes the notations. Löwner matrices are defined in Section II-B while Section II-C discusses the problem of blind signal separation (BSS). In Section II-D, it is shown how Löwner matrices and tensors can be used in the setting of separating (approximations by) rational functions.

A. Multilinear algebra and notations

1) Tensors and notation: Tensors, denoted by calligraphic letters, e.g., $\mathcal{A}$, are higher-order generalizations of vectors (denoted by boldface lowercase letters, e.g., $\mathbf{a}$) and matrices (denoted by boldface uppercase letters, e.g., $\mathbf{A}$). Scalars are written as italic lowercase letters, e.g., a. The entry with row index i and column index j of a matrix $\mathbf{A} \in \mathbb{C}^{I\times J}$ is denoted by a_{ij}. Likewise, the $(i_1, i_2, \ldots, i_N)$th entry of an Nth-order tensor $\mathcal{A} \in \mathbb{C}^{I_1\times I_2\times \ldots \times I_N}$ is denoted by $a_{i_1 i_2 \ldots i_N}$. The jth column of a matrix $\mathbf{A} \in \mathbb{C}^{I\times J}$ is denoted by $\mathbf{a}_j$. The superscripts $\cdot^{\mathrm{T}}$, $\cdot^{\mathrm{H}}$, $\cdot^{-1}$ and $\cdot^{\dagger}$ represent the transpose, complex conjugated transpose, inverse and pseudo inverse, respectively. The symbol $\otimes$ and $\circ$ denotes the outer product and Hadamard product, respectively.

2) Tensor decompositions: A tensor $\mathcal{T}$ has rank 1 if it can be written as the outer product of some nonzero vectors: $\mathcal{T} = \mathbf{a}^{(1)} \otimes \mathbf{a}^{(2)} \otimes \ldots \otimes \mathbf{a}^{(N)}$. If $\mathcal{T}$ is written as a linear combination of R rank-1 tensors, one obtains a Polyadic Decomposition (PD):

$$\mathcal{T} = \sum_{r=1}^{R} \mathbf{a}_r^{(1)} \otimes \cdots \otimes \mathbf{a}_r^{(N)} \triangleq \left[\!\!\left[\mathbf{A}^{(1)}, \ldots, \mathbf{A}^{(N)} \right]\!\!\right].$$

If R is minimal, the decomposition becomes canonical (CPD) and the rank of $\mathcal{T}$ is defined as R.

Another decomposition is the low multilinear rank approximation (LMLRA) [19]. One way of calculating an LMLRA is through the multilinear singular value decomposition (MLSVD) [20]. A tensor $\mathcal{T}$ can then be written as the tensor-matrix product of a typically smaller core tensor $\mathcal{S}$ with N factor matrices $\mathbf{U}^{(n)}$, $n = 1, \ldots, N$, along the different modes. For more details on tensors and tensor decompositions, we refer the interested reader to [15], [16], [21].

3) Computation of tensor decompositions: Given a tensor $\mathcal{T}$, there are a number of algorithms available to find the rank-1 terms of $\mathcal{T}$. The most popular one is the alternating least squares (ALS) method, whereas a more advanced algorithm is the nonlinear least squares (NLS) method. Two commonly used initialization methods are random initializations and a technique based on the generalized eigenvalue decomposition (GEVD) [22].

The approach in this paper makes use of a compression step and a CPD step [23]. The compression step applies an MLSVD with truncation to compute a smaller core tensor $\mathcal{S}$ and corresponding factor matrices $\mathbf{U}^{(n)}$. Provided that the dimensions of $\mathcal{S}$ exceed R, it can be shown that $\mathcal{S}$ still has (approximately) rank R if $\mathcal{T}$ has (approximately) rank R. In the second step, a CPD is performed on the smaller tensor $\mathcal{S}$ (rather than on $\mathcal{T}$), which returns the factor matrices $\mathbf{B}^{(n)}$. The nth factor matrix of $\mathcal{T}$ is then equal to $\mathbf{A}^{(n)} = \mathbf{U}^{(n)}\mathbf{B}^{(n)}$. This two-step procedure is especially beneficial if $\mathcal{T}$ is large, as the computation complexity of CPD algorithms is higher compared to the MLSVD algorithms. If $\mathcal{T}$ only approximately has rank R, the two-step procedure still provides good estimates in various occasions which differ only minimally compared to the estimates from computing a CPD on $\mathcal{T}$ directly.

B. Löwner matrices and tensors

While the concept of Löwner matrices is highly acknowledged in the domain of system identification [24], [25], it is not well known in other application domains. In a recent study, Löwner matrices have been used in a BSS context to separate (approximations by) rational functions [14].

Suppose a function $f(t) \in \mathbb{C}$ is given, evaluated in the point set $T = \{t_1, t_2, \ldots, t_N\}$. The point set T is partitioned into two distinct point sets, $X = \{x_1, x_2, ..., x_I\}$ and $Y = \{y_1, y_2, ..., y_J\}$ with $I + J = N$. The elements of the Löwner matrix $\mathbf{L} \in \mathbb{C}^{I\times J}$ are then defined as

$$\forall i, j: \quad l_{ij} = \frac{f(x_i) - f(y_i)}{x_i - y_j}.$$

We thus obtain the following matrix:

$$\mathbf{L} = \begin{bmatrix} \frac{f(x_1)-f(y_1)}{x_1-y_1} & \frac{f(x_1)-f(y_2)}{x_1-y_2} & \cdots & \frac{f(x_1)-f(y_J)}{x_1-y_J} \\ \frac{f(x_2)-f(y_1)}{x_2-y_1} & \frac{f(x_2)-f(y_2)}{x_2-y_2} & \cdots & \frac{f(x_2)-f(y_J)}{x_2-y_J} \\ \vdots & \vdots & \ddots & \vdots \\ \frac{f(x_I)-f(y_1)}{x_I-y_1} & \frac{f(x_I)-f(y_2)}{x_I-y_2} & \cdots & \frac{f(x_I)-f(y_J)}{x_I-y_J} \end{bmatrix}.$$

Given K functions $f_i(t)$ evaluated on the same set of N points, a Löwner matrix $\mathbf{L}_i$ can be computed for each function. By stacking the different matrices $\mathbf{L}_i$ in a tensor along the third mode, a Löwner tensor $\mathcal{L} \in \mathbb{C}^{I\times J\times K}$ is obtained.

C. Blind signal separation

Given a set of observed signals $\mathbf{S} \in \mathbb{C}^{N\times K}$, the BSS problem consists of identifying the mixing matrix $\mathbf{H} \in \mathbb{C}^{K\times R}$ and/or the original source signals in $\mathbf{W} \in \mathbb{C}^{N\times R}$ based on the following linear model:

$$\mathbf{S} = \mathbf{W}\mathbf{H}^{\mathrm{T}}, \tag{1}$$

with K the number of observed signals, R the number of source signals and N the number of samples per signal. By itself, the solution cannot be uniquely identified as different working hypotheses lead to different solutions (at least for the non-trivial cases $R > 1$). Different working assumptions have been used before such as mutual independence of the source signals which leads to independent component analysis. In this paper, we use a deterministic approach with the assumption that each source can be well approximated by a rational function as discussed in the next section.

D. Löwner-based blind signal separation of (approximations by) rational functions

Rational functions are formed by algebraic fractions with polynomials in the numerator and denominator. We limit the discussion in this paper to rational functions of degree 1, meaning that the numerator and denominator are linear functions. This is a special case of the technique developed in [14] for arbitrary degree.

If $\mathbf{L}$ is a Löwner matrix constructed by a rational function of degree 1, it has been proven that $\mathbf{L}$ has rank 1 [24], [26]. This is easy to verify: $f(t) = \frac{c}{t-p}$ gives $L_{i,j} = -c \cdot \frac{1}{x_i - p} \cdot \frac{1}{y_j - p}$, which is a rank-1 structure:

$$\mathbf{L} = -c \cdot \begin{bmatrix} \frac{1}{x_1 - p} \\ \vdots \\ \frac{1}{x_I - p} \end{bmatrix} \begin{bmatrix} \frac{1}{y_1 - p} & \cdots & \frac{1}{y_J - p} \end{bmatrix}.$$

Consider now the construction of two tensors $\mathcal{L}_{\mathbf{S}} \in \mathbb{C}^{I \times J \times K}$ and $\mathcal{L}_{\mathbf{W}} \in \mathbb{C}^{I \times J \times N}$. The tensors $\mathcal{L}_{\mathbf{S}}$ and $\mathcal{L}_{\mathbf{W}}$ contain Löwner matrices along the third mode constructed from the observed signals from $\mathbf{S}$, and the source signals from $\mathbf{W}$, respectively. Following the linear model (1), the tensor $\mathcal{L}_{\mathbf{S}}$ can be expressed as

$$\mathcal{L}_{\mathbf{S}} = \sum_{r=1}^{R} \mathbf{L}_{\mathbf{w}_r} \otimes \mathbf{h}_r. \tag{2}$$

If each source signal is an evaluated rational function (or can be approximated by an evaluated rational function), each matrix $\mathbf{L}_{\mathbf{w}_r}$ has (approximately) rank 1 [14]. Hence, each term in (2) has (approximately) rank 1 and the tensor $\mathcal{L}_{\mathbf{S}}$ has CPD structure with rank R.

To solve the BSS problem from (1) under the deterministic assumption of rationality, a CPD can be computed of $\mathcal{L}_{\mathbf{S}}$ with rank R. The factor matrix $\hat{\mathbf{H}}$ in the third mode is then an estimate of the mixing matrix $\mathbf{H}$. The source signals can be recovered as $\hat{\mathbf{W}} = \mathbf{S}\left(\hat{\mathbf{H}}^{\mathrm{T}}\right)^{\dagger}$. Alternatively, estimates of the source signals can be obtained from the estimated matrices $\hat{\mathbf{L}}_{\mathbf{w}_r}$. Note that the two indeterminacies of BSS are consistent with the indeterminacies of the CPD: the source signals (factor vectors) are recovered up to permutation and scaling.

It remains to show that the separation is unique, i.e., the recovered source signals are (estimates of) the original source signals. This uniqueness problem boils down to the CPD uniqueness given the special rational structure of the factor vectors. In [14, Theorem 4], it has been proven that if the poles of the rational functions of the different source signals are distinct and if N is sufficiently large, the CPD is unique (up to permutation and scaling of the factor vectors) given that $\mathbf{H}$ does not contain proportional columns. Note that uniqueness can still be guaranteed for underdetermined mixtures with fewer observed signals than source signals. Generic conditions for the BSS settings are given in [27].

III. Löwner-based method for water removal

Section III-A explains the MRSI and the water signal model. Section III-B discusses blind source separation of MRSI signals and in Section III-C, estimation of source parameters obtained from BSS is explained. Section III-D describes the extraction of the water component from the MRSI data.

A. MRSI and residual water

The MRSI time-domain signal is represented by a free-induction decay of the MR signal. The complex time-domain FID signal in each voxel can be modeled by a sum of complex damped exponentials:

$$S(t) = \sum_{r=1}^{R} a_r e^{j\phi_r} e^{(-d_r + j2\pi f_r)t},$$

in which R is the number of resonance peaks in the signal, and f_r, a_r, ϕ_r and d_r are the frequency, amplitude, phase and damping of the r^{th} resonance peak, respectively. Similarly, in the frequency domain, the Fourier transform of the FID signal can be modeled as a sum of rational functions.

$$\begin{aligned} S(f) &= \sum_{r=1}^{R} \frac{a_r e^{j\phi_r}/2\pi}{d_r + j2\pi(f - f_r)} \\ &= \sum_{r=1}^{R} \frac{c_r}{j\omega + p_r} \end{aligned}, \tag{3}$$

where $c_r = a_r e^{j\phi_r}/2\pi$ is the complex amplitude, $p_r = d_r - j2\pi f_r$ is the complex pole and $\omega = 2\pi f$ is the angular frequency.

The MRSI data matrix $\mathbf{S}$ is constructed by stacking the spectra from each voxel in the columns of $\mathbf{S}$. The residual water present in the MRSI signals are sometimes large and can strongly affect the metabolite peaks of interest, which belong to the region of interest in 0.25-4.2 ppm as shown in Fig. 1. In theory, the water signal can be represented by only one exponential/rational function in time/frequency domain, but it is not sufficient for an in-vivo signal. In practice, it is possible to model the residual water signal with a linear combination of several exponentials [7], which can then be extracted from $\mathbf{S}$.

B. Löwner-based blind signal separation in MRSI

Each voxel spectrum is assumed to contain the same resonance peaks as described in (3) but with different corresponding complex amplitudes. Hence, the separation of R individual metabolite signals with their corresponding abundances from the K measured MRSI signals can be formulated as a BSS problem:

$$\mathbf{S} = \mathbf{W}\mathbf{H}^{\mathrm{T}},$$

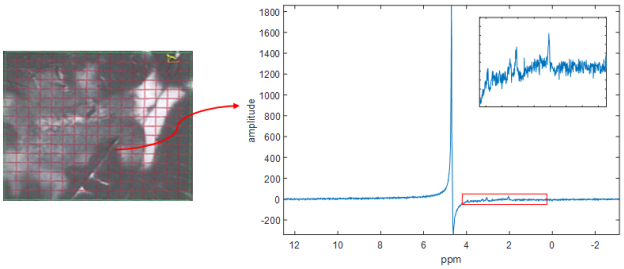


Fig. 1: Magnitude of the absorption spectra from one of the voxels in the MRSI grid with a large residual water signal. The region of interest for metabolites is shown within the red box.

where columns of $\mathbf{S} \in \mathbb{C}^{N\times K}$ contain the measured spectra from all the voxels, the columns of $\mathbf{W} \in \mathbb{C}^{N\times R}$ represent the individual metabolite components and the columns of $\mathbf{H} \in \mathbb{C}^{K\times R}$ (the mixing matrix) represent their corresponding abundances (weights) in each voxel. We use the Löwner-based BSS technique explained in Section II-D to estimate the individual metabolite sources. For each voxel, a Löwner matrix $\mathbf{L}_{\mathbf{s}_k}$ is constructed from the corresponding spectrum in the MRSI grid:

$$\mathbf{L}_{\mathbf{s}_k} = \begin{bmatrix} \frac{\mathbf{s}_k(x_1)-\mathbf{s}_k(y_1)}{x_1-y_1} & \frac{\mathbf{s}_k(x_1)-\mathbf{s}_k(y_2)}{x_1-y_2} & \cdots & \frac{\mathbf{s}_k(x_1)-\mathbf{s}_k(y_J)}{x_1-y_J} \\ \frac{\mathbf{s}_k(x_2)-\mathbf{s}_k(y_1)}{x_2-y_1} & \frac{\mathbf{s}_k(x_2)-\mathbf{s}_k(y_2)}{x_2-y_2} & \cdots & \frac{\mathbf{s}_k(x_2)-\mathbf{s}_k(y_J)}{x_2-y_J} \\ \vdots & \vdots & \ddots & \vdots \\ \frac{\mathbf{s}_k(x_I)-\mathbf{s}_k(y_1)}{x_I-y_1} & \frac{\mathbf{s}_k(x_I)-\mathbf{s}_k(y_2)}{x_I-y_2} & \cdots & \frac{\mathbf{s}_k(x_I)-\mathbf{s}_k(y_J)}{x_I-y_J} \end{bmatrix},$$

in which $\mathbf{s}_k$ is the spectrum of the kth voxel, and with $\{x_1, ..., x_I\}$ and $\{y_1, ..., y_I\}$ two partitions of the point set $\Omega = \{\omega_1, \ldots, \omega_N\}$ with $N = I + J$. Two typical partitioning types for Ω are interleaved and block partitioning. Interleaved partition was used for constructing Löwner matrix in this paper.

The Löwner matrix is constructed using the spectrum from 0.25-6.5 ppm, which contains the region of interest in 0.25-4.2 ppm and the water region. A third-order tensor $\mathcal{L}_{\mathbf{S}}$ is obtained by stacking the Löwner matrices along the third mode as shown in Fig. 2.

As it is assumed that each individual component $\mathbf{w}_r$ can be well approximated by a degree-1 rational function with a single resonance peak as described in (3), each corresponding rth Löwner matrix has approximately rank 1 and can be described as $\mathbf{a}_r\mathbf{b}_r^{\mathsf{T}}$. Hence, a CPD can be applied on $\mathcal{L}_{\mathbf{S}}$:

$$\mathcal{L}_{\mathbf{S}} \approx \sum_{r=1}^{R} \mathbf{a}_r \otimes \mathbf{b}_r \otimes \mathbf{h}_r = [\![\mathbf{A}, \mathbf{B}, \mathbf{H}]\!], \tag{4}$$

with $\mathbf{A} \in \mathbb{C}^{I\times R}$, $\mathbf{B} \in \mathbb{C}^{J\times R}$ and $\mathbf{H} \in \mathbb{C}^{K\times R}$. Each rank-1 tensor corresponds to the contribution of a particular component to the observed spectral data.

C. Estimation of source parameters

The abundance vectors $\mathbf{h}_r$ can be directly identified from (4). A second goal is to identify the source components and their corresponding parameters as described in (3). The rth source is modeled by $\mathbf{w}_r(\omega) = \frac{c_r}{j\omega+p_r}$, and its corresponding Löwner matrix $\mathbf{L}_{\mathbf{w}_r}$ can be written as:

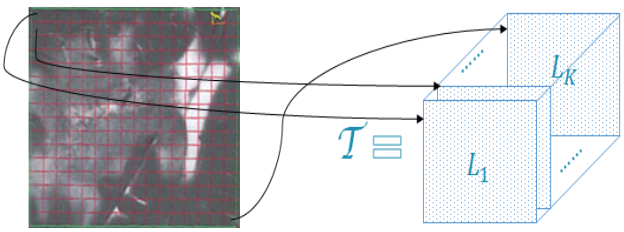


Fig. 2: Construction of the Löwner tensor $\mathcal{T}$ from the spectra of the different MRSI voxels

$$\mathbf{L}_{\mathbf{w}_r} = \begin{bmatrix} \frac{-jc_r}{(jx_1+p_r)(jy_1+p_r)} & \frac{-jc_r}{(jx_1+p_r)(jy_2+p_r)} & \cdots & \frac{-jc_r}{(jx_1+p_r)(jy_J+p_r)} \\ \frac{-jc_r}{(jx_2+p_r)(jy_1+p_r)} & \frac{-jc_r}{(jx_2+p_r)(jy_2+p_r)} & \cdots & \frac{-jc_r}{(jx_2+p_r)(jy_J+p_r)} \\ \vdots & \vdots & \ddots & \vdots \\ \frac{-jc_r}{(jx_I+p_r)(jy_1+p_r)} & \frac{-jc_r}{(jx_I+p_r)(jy_2+p_r)} & \cdots & \frac{-jc_r}{(jx_I+p_r)(jy_J+p_r)} \end{bmatrix}$$

$$= \begin{bmatrix} \frac{c_r^{(1)}}{jx_1+p_r} \\ \frac{c_r^{(1)}}{jx_2+p_r} \\ \vdots \\ \frac{c_r^{(1)}}{jx_I+p_r} \end{bmatrix} \begin{bmatrix} \frac{c_r^{(2)}}{jy_1+p_r} & \frac{c_r^{(2)}}{jy_2+p_r} & \cdots & \frac{c_r^{(2)}}{jy_J+p_r} \end{bmatrix}$$

$$= \mathbf{a}_r\mathbf{b}_r{}^{\mathsf{T}}$$

with $-jc_r = c_r^{(1)}c_r^{(2)}$. The parameters $c_r^{(1)}$ and p_r can be obtained from $\mathbf{a}_r$ using least squares,

$$\begin{bmatrix} p_r \\ c_r^{(1)} \end{bmatrix} = \begin{bmatrix} \mathbf{a}_r & -\mathbf{1} \end{bmatrix}^{\dagger} (j\mathbf{x} \circ \mathbf{a}_r),$$

where $\mathbf{1} \in \mathbb{R}^I$ is the vector with all ones. We can estimate $c_r^{(2)}$ and p_r from $\mathbf{b}_r$ in a similar way. The final estimate of p_r can be obtained by averaging the estimates from $\mathbf{a}_r$ and $\mathbf{b}_r$.

D. Water signal suppression

Once the source parameters are estimated, the model is extrapolated to the entire length of the frequency region. The abundance matrix $\mathbf{H}$ is calculated using least squares from the source signals and measured spectra, $\mathbf{H} = (\mathbf{W}^{\dagger}\mathbf{S})^{\mathsf{T}}$. The real part of each estimated pole gives the damping factor of the corresponding source (d_r) while the imaginary part returns the resonance frequency. The components whose resonance frequencies are outside the region of interest (0.25 - 4.2 ppm) belong to the water component or provide other nuisance peaks. Therefore, the influence of the water component on the observed spectral data is constructed using only those components and their corresponding abundance vectors. Let Φ denote the set of P indices corresponding to the P water parts. Then $\mathbf{W}_{water} = \begin{bmatrix} \mathbf{w}_{\Phi_1} & \cdots & \mathbf{w}_{\Phi_P} \end{bmatrix}$ and $\mathbf{H}_{water} = \begin{bmatrix} \mathbf{h}_{\Phi_1} & \cdots & \mathbf{h}_{\Phi_P} \end{bmatrix}$, and the contribution of the water component can be expressed as $\mathbf{S}_{water} = \mathbf{W}_{water}\mathbf{H}_{water}^{\mathsf{T}}$. The water component can then be removed from the measured MRSI spectra as $\mathbf{S}_{suppressed} = \mathbf{S} - \mathbf{S}_{water}$.

After removing the water component from the MRSI signal, a small baseline will be present at the outer edges of the spectrum. This may arise because we only consider spectra in the region 0.25-6.5 ppm for constructing the Löwner matrices. Second, the model containing the sum of degree-1 rational functions may not be able to model the complex water signal properly. This problem can be rectified by modeling the baseline using a polynomial function of degree D. Therefore, the polynomial functions are added to the estimated source matrix $\mathbf{W}$ to obtain the matrix $\mathbf{W}_{poly} \in \mathbb{R}^{N\times(K+d+1)}$:

$$\mathbf{W}_{poly} = \begin{bmatrix} w_{11} & w_{12} & \dots & w_{1R} & 1 & f_1 & f_1^2 & \dots & f_1^d \\ w_{21} & w_{22} & \dots & w_{2R} & 1 & f_2 & f_2^2 & \dots & f_2^d \\ \vdots & \vdots & \ddots & \vdots & \vdots & \vdots & \vdots & \ddots & \vdots \\ w_{N1} & w_{N2} & \dots & w_{NR} & 1 & f_N & f_N^2 & \dots & f_N^d \end{bmatrix}$$

The abundance matrix $\mathbf{H}$ is recalculated in a least-square sense using the estimate of $\mathbf{W}_{poly}$ and the measured spectra in $\mathbf{S}$. The residual water component is suppressed using the subtraction method as explained above. Each polynomial source is also considered as a water component.

The CPD algorithm requires an initial value for the factor matrices. Random initializations can sometimes result in poor water suppression. In order to overcome this problem, different initializations are used if the water suppression is not sufficient. To verify the quality of the water suppression, the variance in the water region and noise region are compared. If the variance in the water segment is larger than the variance in the noise segment by a given threshold, the water suppression is considered to be poor and a different initial value is used until a good suppression is obtained.

IV. Results

To test the performance of the Löwner-based water suppression method, it is applied on both simulated and in-vivo MRSI data. Section IV-A discusses the performance of the Löwner and HSVD method on two simulated datasets. In Section IV-B the performance measure for in-vivo data is described along with the results of the Löwner and HSVD method. Tensorlab is used for the Löwner matrix constructions and tensor computations [28], [29]. The signal-to-noise ratio (SNR) is defined as the power of the signal to the power of the noise. Unless stated otherwise, a rank $R = 50$ is used for the CPD of the Löwner tensor $\mathcal{L}_{\mathbf{S}}$ for both the simulated and in-vivo cases. For the HSVD, an order of 25 was used.

A. Simulations

The simulated signals containing residual water are generated using an in-vitro basis set. The basis set consisted of in-vitro signals from Alanine (Ala), Aspartate (Ala), Choline (Cho), Creatine (Cre), γ-aminobutyric acid (GABA), Glutamate (Glu), Lactate (Lac), two lipids (Lip1 and Lip2), myo-Inositol (MI), N-Acetyl-Aspartate (NAA) and Taurine (Tau) metabolites. A grid of MRSI signals of size 16×16 was generated for simulation. First, signals consisting of 12 metabolites are constructed using the basis set without any residual water. The amplitude of each metabolite in the grid is varied using a 2-D Gaussian window,

$$g(x, y) = e^{-(x^2+y^2)/2\sigma^2} + U(x, y)$$

where $U(x, y)$ is a uniformly distributed random number, and $x = 0$, $y = 0$ is the central voxel. Circular Gaussian noise is added to the metabolite signals. The estimated water component using HSVD or the Löwner method obtained from in-vivo MRSI measurements are used as residual water signal in the simulations, which are linear combinations of damped sinusoids. The residual water signals are added to the noisy metabolite signals to generate the MRSI data. The Löwner and HSVD water-suppression methods are applied on the simulated MRSI signals for 100 different noise and metabolite amplitude realizations.

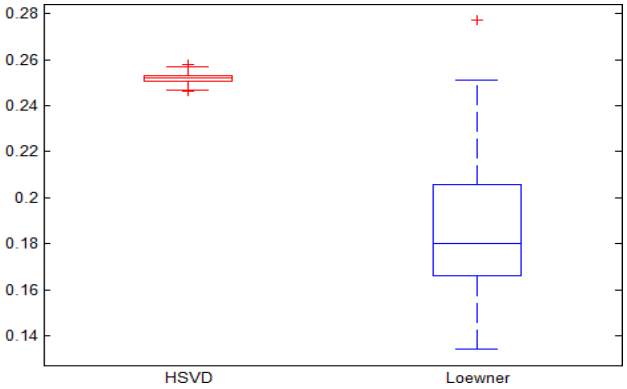


Fig. 3: Boxplots of residual error after water suppression using the HSVD and the Löwner method without polynomial on 100 simulated in-vitro MRSI signals. The error is calculated as the l_2-norm of difference between the water-suppressed signal and the original one without water signal. A simple water model without any distortion was used in simulation.

Fig. 3 shows the boxplot of error between the water-suppressed signal and the metabolite signal (with noise). The boxplot indicates that the Löwner-based method has a lower average error compared to the HSVD, and suppresses the residual water better without distorting the metabolite spectra.

In the second simulation the residual water signal is distorted by multiplying it with an exponentially decaying signal. The HSVD and Löwner methods are applied on the simulated signals to suppress the water. The real part of the water-suppressed spectrum is shown in Fig. 4 along with the original signal for one voxel in the MRSI grid. From Fig. 4 it is clear that the Löwner method with polynomial sources performs better than the Löwner method without polynomial sources by avoiding the baseline at the outer edges of the spectrum.

The simulation is run 100 times with two different SNR values. Fig. 5 shows the residual errors for the water-free simulated MRSI signal and the water-suppressed MRSI signal obtained from the HSVD and Löwner methods.

B. In-vivo results

A total of 28 2-D-^{1}H MRSI data was acquired on a 3T MR scanner (Achieva, Philips, Best, The Netherlands) at the

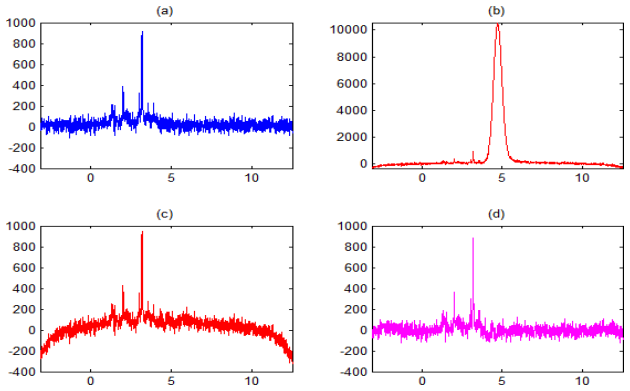


Fig. 4: (a) Absorption spectrum of a simulated in-vitro signal without water from one of the MRSI voxels. (b) Absorption spectrum of a simulated in-vitro signal with large water peak from one of the MRSI voxels. (c) Absorption spectrum of the water-suppressed signal using the Löwner method without polynomial sources. (d) Absorption spectrum of the water-suppressed signal using the Löwner method with polynomial sources.

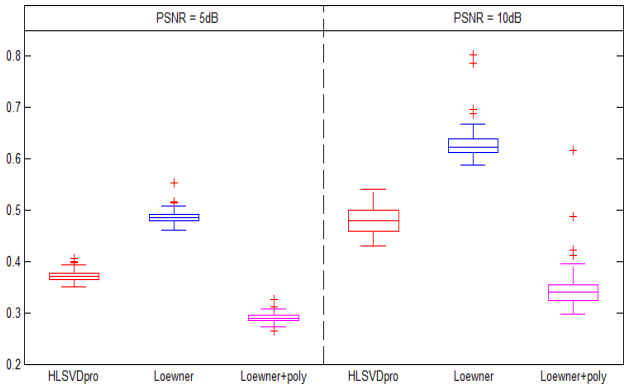


Fig. 5: Boxplot of the residual errors after water suppression using the HSVD method and Löwner methods without and with polynomial components on 100 simulated in-vitro MRSI signals. The error is calculated as the l_2-norm of the difference between the water-suppressed signal and the original water-free signal. In the simulation, the residual water is distorted by multiplication with the exponential signal.

University Hospital of Leuven using the following protocol [30]: a point-resolved spectroscopy (PRESS) sequence was used as the volume selection technique with a bandwidth of 1.3kHz for the conventional slice-selective pulses; repetition time (TR)/ echo time (TE): 2000/35ms; Field of view (FOV): 160×160mm^2; maximal volume of interest (VOI): 80×80mm^2; slice thickness: 10mm; acquisition voxel size: 10×10mm^2; reconstruction voxel size: 5×5mm^2; receiver bandwidth: 2000Hz; samples: 2048; number of signal averages: 1; water suppression method: multiple optimizations insensitive suppression train [6]; first- and second-order pencil beam shimming; parallel imaging: sensitivity encoding with reduction factors of 2 (left-right) and 1.8 (anterior-posterior); scan time: around 3min 30s. Automated prescanning optimized the shim in order to yield a peak width consistently under

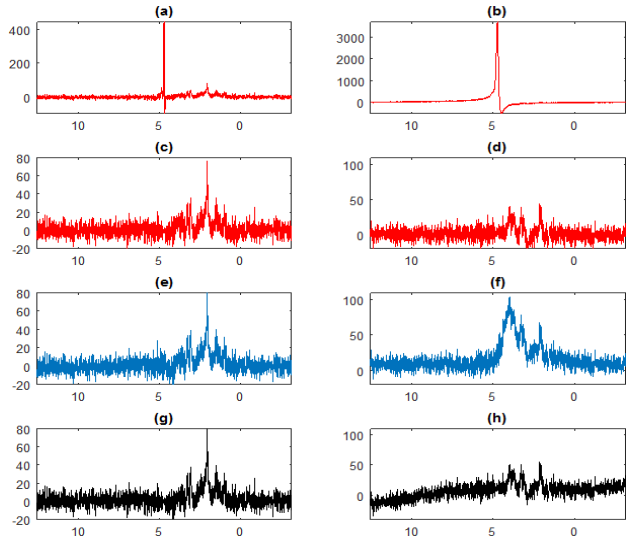


Fig. 6: Residual water suppression in in-vivo MRSI signal. (a-b) Absorption spectra of measured MRSI signal with large residual water peak for two voxels. (c-d) Absorption spectrum of the water-suppressed signal using the Löwner method with polynomial in the two corresponding voxels. (e-f) Absorption spectrum of the water-suppressed signal using HSVD method in the two corresponding voxels. (g-h) Absorption spectrum of the water-suppressed signal using the Löwner method without polynomial in the two corresponding voxels.

20Hz full-width half-maximum (FWHM). The study and the experimental procedures involving human subjects have been approved by the ethical committee of the institute.

To test the performance of the algorithms we have applied the HSVD and Löwner methods on 28 in-vivo datasets. Fig. 6 shows the real part of the spectra with residual water and after water suppression for two different voxels in a MRSI grid. In many voxels, all three methods give good water suppression as shown in Fig. 6c. However, in some voxels the HSVD method does not perform well as shown in Fig. 6f. The Löwner method without polynomial source components can introduces a baseline at the spectral edges as shown in Fig. 6h.

There is no ground truth available for in-vivo data to measure the quality of water suppression. To measure the performance, we calculate the difference in sample variance between the water region segment and the noise segment in each voxel. The spectrum in the region of 4.2-5.2 ppm is considered as water segment and the spectrum at the outer edges is considered as noise segment. For each MRSI signal, the average difference in variance is used as the performance measure. Fig. 7 shows the boxplot of sample variance difference of 28 MRSI in-vivo data signals for the HSVD and Löwner methods.

V. Discussion

Residual water suppression is one of the common preprocessing steps used in the quantification of MRSI signals. In the filtering-based method by T. Sundin et. al. [13], a maximum-phase finite impulse response filter is used for the residual water suppression. This method will alter the amplitude and

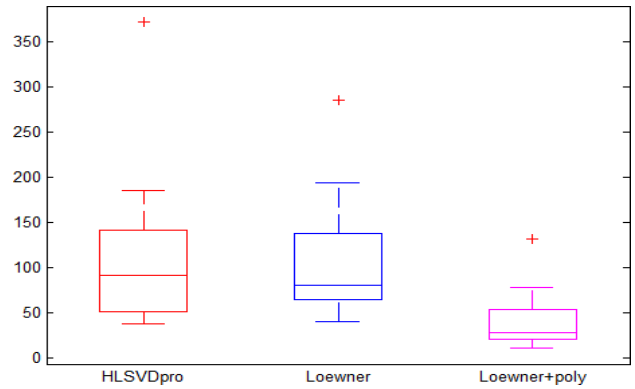


Fig. 7: Boxplots of error after residual water suppression using the methods HSVD, Löwner without polynomial and Löwner with polynomial in 28 in-vivo MRSI signals. The error is calculated as the difference between the variance in water region segment and the variance from a segment in the noise region.

phase of the filtered signal, which may create problems in quantification methods where different phase variations are not allowed and where spectra instead of quantified metabolites are used for the analysis [31], [32]. HSVD is the most widely used method and is available as a preprocessing step in many MRSI software packages. As it is applied on a voxel-by-voxel basis and as it separates the water source components separately for each voxel, it does not exploit the information shared among the voxels in the MRSI grid. Therefore, the HSVD method can fail to suppress water completely in a particular voxel due to noise or artifacts present in that voxel. This problem can be seen in an in-vivo example shown in Fig. 6 where the HSVD method fails to suppress the water in a particular voxel (Fig. 6f) and performs better in another voxel (Fig. 6e). This has motivated us to develop a new algorithm, which can exploit the similarity in water sources present among all voxels.

In this paper, we have represented the second-order MRSI data using a third-order tensor by means of a Löwner transform. A novel residual water-suppression method based on the CPD where sources are shared among all voxels was developed. This work explored the feasibility and efficiency of the proposed algorithm in suppressing the residual water from MRSI data using both simulation and in-vivo signals. The Löwner-based method is applied simultaneously on the entire MRSI grid to estimate the sources, which are shared by all the voxels. The water signal in each voxel is estimated as the linear combination of the sources with different weights. This helps in preventing the failure of the water suppression in single voxels.

The Löwner tensor is constructed using truncated spectra. Only the parts where the metabolite and water peaks are present are retained in the spectra. This helps in reducing the size of the tensor and the computational complexity of the algorithm. One of the interesting properties of the Löwner-based BSS method is that the point sets X and Y used in the construction of the Löwner matrix do not need to be uniform. In this way, we can apply the Löwner-based BSS using the entire spectrum without drastically increasing the computational time compared to truncated spectra by using all the points in the region of interest and only a few points from the remaining region. Empirical results show that the water-suppressing performance is similar to when using the truncated spectra, while the baseline will also be present when no additional polynomial source components are used.

To estimate the water sources we have applied the CPD only on the compressed core tensor S and the factor matrices are obtained as explained in the Section II-A. It speeds up the algorithm without any significant negative consequences in the estimated water signal. The factor matrices obtained from the compressed CPD step are typically used as the initial values in the computation of the CPD of the full tensor, also known as the refinement step. Here, we have completely skipped the refinement step as it is computationally intensive and did not provide any significant improvement in the estimated water signal. In the Löwner-based method we have added a quality verification on the water suppression to overcome the problems with random initialization. If the algorithm is used with different initializations to obtain a better water suppression, the compression step is only performed once as it is deterministic. Since the compression step takes most of the computation time and the CPD on the core tensor is relatively fast, running the algorithm again with a different initialization will not increase the computation significantly. A rank $R = 50$ was used for the CPD of the Löwner tensor $\mathcal{L}_{\mathbf{S}}$ based on the assumption that the water signal from all the voxels can be modelled using 10-15 first-order rational functions and the remaining are sufficient to model the metabolites. The chosen rank performs similarly on the larger voxel grid (16×16) and as well as on the smaller voxel grid (8×8). Also the selection of rank is not sensitive and the results does not deviate much if a rank of 40 or 60 was selected.

VI. Conclusion

A tensor-based method which suppresses residual water simultaneously in all MRSI voxels using a Löwner-based blind source separation technique is proposed. This method was tested on both simulated and in-vivo ^{1}H MRSI signals. In the case that a simple water model is used in the simulations, the Löwner method performs better than the widely-used subspace-based HSVD method, which uses a single Hankel matrix from one spectrum at a time. When the water signal is distorted using a decaying exponential in the simulated signals, the basic Löwner method introduces some baseline at the outer edges. The Löwner method with polynomial source components can handle this problem better, and performs better than the HSVD method. Regarding the in-vivo ^{1}H MRSI data, both basic Löwner and HSVD methods had a similar performance, while the Löwner method with polynomial source components performed significantly better in suppressing the residual water signal.

Acknowledgment

The authors would like to thank the University Hospitals of Leuven for data acquisition.

REFERENCES

[1] S. R. Dager, N. Oskin, T. L. Richards, and S. Posse, "Research applications of magnetic resonance spectroscopy (MRS) to investigate psychiatric disorders," *Topics in magnetic resonance imaging: TMRI*, vol. 19, no. 2, p. 81, 2008.

[2] F. S. De Edelenyi, A. Simonetti, G. Postma, R. Huo, and L. Buydens, "Application of independent component analysis to ^{1}H MR spectroscopic imaging exams of brain tumours," *Analytica Chimica Acta*, vol. 544, no. 1, pp. 36–46, 2005.

[3] S. Van Cauter, F. De Keyzer, D. M. Sima, Croitor Sava A. R., F. D'Arco, J. Veraart, R. R. Peeters, A. Leemans, S. Van Gool, G. Wilms, P. Demaerel, S. Van Huffel, S. Sunaert, and U. Himmelreich, "Integrating diffusion kurtosis imaging, dynamic susceptibility-weighted contrast-enhanced MRI, and short echo time chemical shift imaging for grading gliomas," *Neuro-oncology*, vol. 16, no. 7, pp. 1010–1021, 2014.

[4] P. J. Bolan, M. T. Nelson, D. Yee, and M. Garwood, "Imaging in breast cancer: magnetic resonance spectroscopy," *Breast Cancer Research*, vol. 7, no. 4, p. 1, 2005.

[5] S. Friedman, D. Shaw, A. Artru, T. Richards, J. Gardner, G. Dawson, S. Posse, and S. Dager, "Regional brain chemical alterations in young children with autism spectrum disorder," *Neurology*, vol. 60, no. 1, pp. 100–107, 2003.

[6] R. J. Ogg, R. Kingsley, and J. S. Taylor, "WET, a T1-and B1-insensitive water-suppression method for in vivo localized ^{1}H NMR spectroscopy," *Journal of Magnetic Resonance, Series B*, vol. 104, no. 1, pp. 1–10, 1994.

[7] E. Cabanes, S. Confort-Gouny, Y. Le Fur, G. Simond, and P. J. Cozzone, "Optimization of residual water signal removal by HLSVD on simulated short echo time proton MR spectra of the human brain," *Journal of Magnetic Resonance*, vol. 150, no. 2, pp. 116–125, 2001.

[8] L. Vanhamme, R. D. Fierro, S. Van Huffel, and R. de Beer, "Fast removal of residual water in proton spectra," *Journal of Magnetic Resonance*, vol. 132, no. 2, pp. 197–203, 1998.

[9] D. Stefan, F. Di Cesare, A. Andrasescu, E. Popa, A. Lazariev, E. Vescovo, O. Strbak, S. Williams, Z. Starcuk, M. Cabanas *et al.*, "Quantitation of magnetic resonance spectroscopy signals: the jMRUI software package," *Measurement Science and Technology*, vol. 20, no. 10, p. 104035, 2009.

[10] J. B. Poullet, "Quantification and classification of magnetic resonance spectroscopic data for brain tumor diagnosis," Ph.D. dissertation, PhD Thesis. Leuven, Belgium, 2008.

[11] B. Soher, P. Semanchuk, D. Todd, J. Steinberg, and K. Young, "VeSPA: integrated applications for RF pulse design, spectral simulation and MRS data analysis," in *Proceedings of 19th Annual Meeting ISMRM*, 2011, p. 1410.

[12] M. Wilson, G. Reynolds, R. A. Kauppinen, T. N. Arvanitis, and A. C. Peet, "A constrained least-squares approach to the automated quantitation of in vivo ^{1}H magnetic resonance spectroscopy data," *Magnetic resonance in medicine*, vol. 65, no. 1, pp. 1–12, 2011.

[13] T. Sundin, L. Vanhamme, P. Van Hecke, I. Dologlou, and S. Van Huffel, "Accurate quantification of ^{1}H spectra: From finite impulse response filter design for solvent suppression to parameter estimation," *Journal of Magnetic Resonance*, vol. 139, no. 2, pp. 189–204, 1999.

[14] O. Debals, M. Van Barel, and L. De Lathauwer, "Löwner-Based Blind Signal Separation of Rational Functions With Applications," *Signal Processing, IEEE Transactions on*, vol. 64, no. 8, pp. 1909–1918, April 2016.

[15] A. Cichocki, D. Mandic, L. De Lathauwer, G. Zhou, Q. Zhao, C. Caiafa, and H. Phan, "Tensor decompositions for signal processing applications: From two-way to multiway component analysis," *Signal Processing Magazine, IEEE*, vol. 32, no. 2, pp. 145–163, March 2015.

[16] N. Sidiropoulos, L. De Lathauwer, X. Fu, K. Huang, E. Papalexakis, and C. Faloutsos, "Tensor Decomposition for Signal Processing and Machine Learning," *Signal Processing, IEEE Transactions on*, to be published.

[17] I. Domanov and L. De Lathauwer, "On the uniqueness of the canonical polyadic decomposition of third-order tensors — Part I: Basic results and uniqueness of one factor matrix," *SIAM Journal on Matrix Analysis and Applications*, vol. 34, no. 3, pp. 855–875, 2013.

[18] ——, "On the uniqueness of the canonical polyadic decomposition of third-order tensors — Part II: Uniqueness of the overall decomposition," *SIAM Journal on Matrix Analysis and Applications*, vol. 34, no. 3, pp. 876–903, 2013.

[19] L. De Lathauwer, B. De Moor, and J. Vandewalle, "On the best rank-1 and rank-$(R_1, R_2, \ldots, R_n)$ approximation of higher-order tensors," *SIAM Journal on Matrix Analysis and Applications*, vol. 21, no. 4, pp. 1324–1342, 2000.

[20] ——, "A multilinear singular value decomposition," *SIAM Journal on Matrix Analysis and Applications*, vol. 21, no. 4, pp. 1253–1278, 2000.

[21] T. G. Kolda and B. W. Bader, "Tensor decompositions and applications," *SIAM review*, vol. 51, no. 3, pp. 455–500, 2009.

[22] E. Sanchez and B. R. Kowalski, "Tensorial resolution: a direct trilinear decomposition," *Journal of Chemometrics*, vol. 4, no. 1, pp. 29–45, 1990.

[23] R. Bro and C. A. Andersson, "Improving the speed of multiway algorithms: Part ii: Compression," *Chemometrics and intelligent laboratory systems*, vol. 42, no. 1, pp. 105–113, 1998.

[24] A. Antoulas and B. Anderson, "On the scalar rational interpolation problem," *IMA Journal of Mathematical Control and Information*, vol. 3, no. 2-3, pp. 61–88, 1986.

[25] T. Antoulas, "A tutorial introduction to the Loewner framework for model reduction," 2014, 9th Elgersburg Workshop Mathematische Systemtheorie.

[26] K. Löwner, "Über monotone matrixfunktionen," *Mathematische Zeitschrift*, vol. 38, no. 1, pp. 177–216, 1934.

[27] I. Domanov and L. De Lathauwer, "Generic uniqueness of a structured matrix factorization and applications in blind source separation," *IEEE Journal of Selected Topics in Signal Processing*, vol. 10, no. 4, pp. 701–711, June 2016.

[28] N. Vervliet, O. Debals, L. Sorber, M. Van Barel, and L. De Lathauwer. (2016, March) Tensorlab 3.0. [Online]. Available: http://www.tensorlab.net

[29] N. Vervliet, O. Debals, and L. De Lathauwer, "Tensorlab 3.0 — Numerical optimization strategies for large-scale constrained and coupled matrix/tensor factorization," 2016, Internal Report 16–173, ESAT–SISTA, KU Leuven (Leuven, Belgium).

[30] S. Van Cauter, D. M. Sima, J. Luts, L. ter Beek, A. Ribbens, R. R. Peeters, M. I. Osorio Garcia, Y. Li, S. Sunaert, S. W. Van Gool *et al.*, "Reproducibility of rapid short echo time CSI at 3 Tesla for clinical applications," *Journal of Magnetic Resonance Imaging*, vol. 37, no. 2, pp. 445–456, 2013.

[31] H. N. Bharath, D. M. Sima, N. Sauwen, U. Himmelreich, L. D. Lathauwer, and S. V. Huffel, "Non-negative canonical polyadic decomposition for tissue type differentiation in gliomas," *IEEE Journal of Biomedical and Health Informatics*, vol. PP, no. 99, pp. 1–1, 2016.

[32] Y. Li, D. M. Sima, S. V. Cauter, Croitor Sava A. R., U. Himmelreich, Y. Pi, and S. Van Huffel, "Hierarchical non-negative matrix factorization (hNMF): a tissue pattern differentiation method for glioblastoma multiforme diagnosis using MRSI," *NMR in Biomedicine*, vol. 26, no. 3, pp. 307–319, 2013.